

A universal linearized subspace refinement framework for neural networks

Wenbo Cao^{a,b,c}, Weiwei Zhang^{a,b,c,*}

^a *School of Aeronautics, Northwestern Polytechnical University, Xi'an 710072, China*

^b *International Joint Institute of Artificial Intelligence on Fluid Mechanics, Northwestern Polytechnical University, Xi'an, 710072, China*

^c *National Key Laboratory of Aircraft Configuration Design, Xi'an 710072, China*

* Correspondence to: aeroelastic@nwpu.edu.cn

Abstract. Neural networks are typically trained using gradient-based methods, yet in many applications their final predictions remain far from the best accuracy attainable within the model's expressive capacity. Here we introduce Linearized Subspace Refinement (LSR), a general and architecture-agnostic framework that exploits the Jacobian-induced linear residual model at a fixed trained network state. By solving the associated residual problem through a reduced direct least-squares formulation, LSR obtains a subspace-optimal solution of the linearized residual model, yielding a refined linear predictor with markedly improved accuracy over standard gradient-trained solutions—without modifying network architectures, loss formulations, or training procedures. Across a range of learning paradigms—including function approximation, data-driven operator learning, and physics-informed operator fine-tuning—we show that the accuracy achieved by gradient-based training often remains far from the attainable accuracy, even when local linearization yields a convex problem, suggesting that loss-induced ill-conditioning can constitute a dominant practical bottleneck, beyond issues of model expressivity or nonconvexity. In contrast, one-shot LSR consistently exposes accuracy levels that are not exploited by standard gradient-based training, often yielding order-of-magnitude error reductions. For operator-constrained problems with composite loss structures, we further introduce Iterative LSR, which alternates one-shot LSR with supervised nonlinear alignment, converting ill-conditioned residual minimization into numerically benign fitting steps and yielding substantially accelerated convergence and improved accuracy. By bridging nonlinear neural representations with reduced-order linear solvers at fixed linearization points, LSR provides a numerically grounded, broadly applicable refinement framework for modern neural networks in supervised learning, operator learning, and scientific computing.

Keywords. Linearized subspace refinement; neural network refinement; Jacobian-based methods; reduced-order solvers; scientific machine learning.

1 Introduction

Neural networks, owing to their expressive power and flexibility [1], are widely used as function approximators in supervised regression, operator learning, and physics-informed scientific computing

[2-5]. In these applications, the objective is often not merely to obtain qualitatively correct predictions, but to approximate continuous solutions or operators with high numerical accuracy. For example, in operator modeling and partial differential equation (PDE) solving, the achievable error magnitude directly determines whether a learned model is suitable for scientific analysis or engineering deployment [2,3]. Consequently, understanding how to systematically extract the highest attainable numerical accuracy from neural networks under fixed architectures and standard training procedures has become a central challenge in scientific machine learning.

From the perspective of classical numerical analysis and linear algebra, ill-conditioning is widely recognized as a primary factor limiting attainable accuracy. Even when a problem is linear or convex in theory, severe ill-conditioning can prevent iterative methods from reaching high-accuracy solutions within a practical computational budget. In contrast, when memory and computational cost permit, direct factorization-based solvers can reliably attain much higher accuracy by bypassing the slow error decay typical to iterative schemes [6,7]. This fundamental distinction underlies long-standing trade-offs between accuracy, stability, and efficiency in numerical computation, and provides a useful lens for re-examining accuracy barriers encountered in neural network models [8].

Despite these insights, modern neural network training remains overwhelmingly dominated by gradient-based iterative optimization [9,10]. In this paradigm, ill-conditioning manifests as slow convergence, training instability, and strong sensitivity to hyperparameter choices, motivating a wide range of increasingly sophisticated optimizers and acceleration strategies, including adaptive learning rates, momentum, quasi-second-order updates, and various forms of preconditioning [11-16]. In parallel, substantial effort has been devoted to improving accuracy in scientific machine learning through architectural inductive biases and problem-specific design choices, encompassing network architectures, sampling strategies, loss reweighting, regularization, curriculum learning, and multi-stage training [2,3,17-23]. While diverse in form, these approaches share a common feature: accuracy improvements are pursued almost exclusively through continued gradient-based updates of the parameter vector θ .

Motivated by these considerations, we formulate a problem setting that is distinct from, yet complementary to, the conventional training paradigm of neural networks. Rather than asking how to further optimize the parameter vector θ through continued gradient-based training, we ask whether—after training has converged and the parameters are fixed at θ_0 —there still exist directions within the locally linearized model induced by the network Jacobian along which the loss can be substantially reduced. More fundamentally, we ask whether direct solvers can be leveraged to bypass the conditioning barriers that limit the attainable accuracy of iterative optimization. Beyond enabling this alternative mode of refinement, this perspective also provides a concrete way to interrogate

attainable accuracy in nonlinear neural networks. For large-scale models, it is generally infeasible to certify whether a trained network has reached a local optimum of the original nonconvex objective, and apparent convergence or small gradients do not constitute reliable optimality guarantees. By contrast, the linearized residual model at a fixed trained state yields a convex least-squares problem whose attainable accuracy—within a Jacobian-induced subspace—can be directly approximated using robust direct solvers. This linearized attainable accuracy therefore serves as an operational and falsifiable probe of how much locally accessible improvement remains unused by standard training, and offers a principled indirect lens for diagnosing accuracy plateaus in nonlinear optimization.

A key observation underlying this perspective is that many seemingly disparate learning tasks share a common objective structure. Supervised regression and classification, data-driven operator learning, and physics-constrained PDE solving can all be formulated as minimizing a residual norm,

$$\min \frac{1}{2} \|\mathbf{f}(\boldsymbol{\theta})\|_2^2,$$

where $\mathbf{f}(\boldsymbol{\theta})$ denotes the residual vector formed by model predictions evaluated at data samples, observation points, or physical constraints. The primary differences among these problems lie in the composition and interpretation of the residuals, rather than in the residual-minimization form itself. This structural universality provides a natural entry point for introducing a unified refinement framework grounded in classical direct solvers.

Linearizing the residual vector around a trained model leads to a classical least-squares problem involving the network Jacobian. However, the Jacobian is typically extremely high-dimensional and dense, rendering direct solves over the full parameter space computationally infeasible. To address this challenge, we introduce the Linearized Subspace Refinement (LSR) framework. LSR constructs a compact correction subspace using highly parallel Jacobian–vector products and computes a subspace-optimal refinement by directly solving a reduced linear residual problem within this subspace. In its one-shot form, LSR operates as a post-training procedure: it does not modify network architectures, loss formulations, or the original training process, yet it can expose substantial additional accuracy that is not exploited by gradient-based training alone under standard training procedures. More broadly, this linearized subspace perspective provides a foundation for both post-training refinement and iterative refinement strategies, which we demonstrate in the following sections across a range of learning paradigms.

2 Results

Method overview

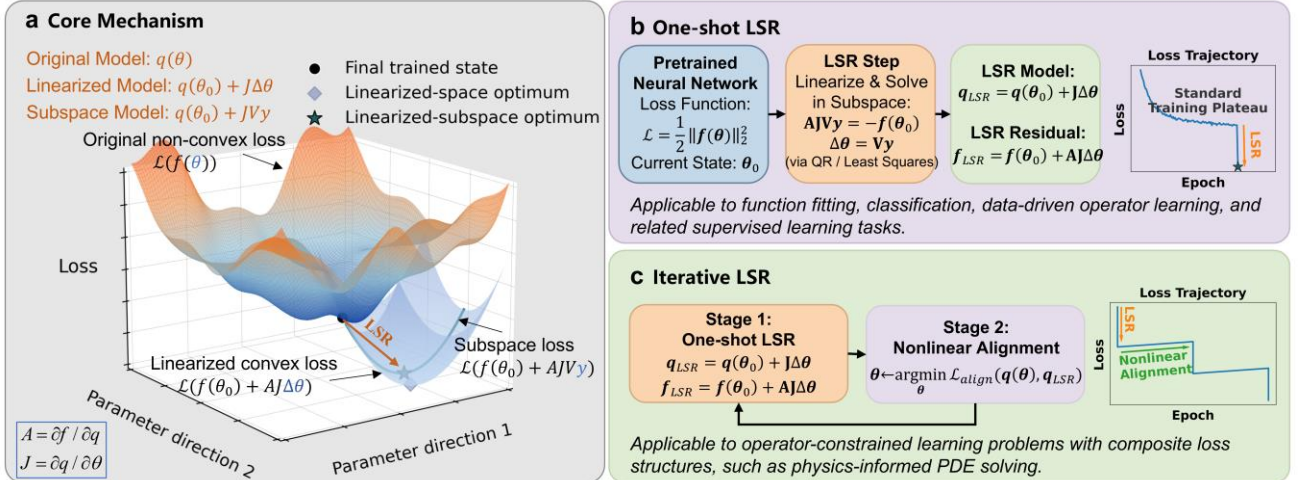


Figure 1 | Overview of the Linearized Subspace Refinement (LSR) framework. a, Core mechanism. Starting from a trained network at parameters θ_0 , the residual vector is locally linearized, inducing a convex least-squares problem with respect to $\Delta\theta$. By restricting $\Delta\theta$ to a low-dimensional subspace, an explicit and computationally tractable direct linear solve yields the optimal correction within this subspace. **b, One-shot LSR.** For function approximation, supervised learning, and data-driven operator learning, a single linearized subspace solve typically suffices to substantially reduce error beyond standard training. **c, Iterative LSR.** For operator-constrained problems with complex composite losses, LSR is alternated with nonlinear alignment, transforming a difficult nonlinear optimization into a sequence of more tractable supervised fitting steps anchored by one-shot LSR solutions, thereby improving both convergence behavior and attainable accuracy. Note: LSR computes $\Delta\theta$ using Jacobian–vector actions evaluated on the training set. Once $\Delta\theta$ is obtained, the refined predictor can be evaluated at any test input x via the corresponding pointwise Jacobian action $J_{\theta_0}(x)\Delta\theta$, yielding $q_{LSR}(x) = q_{\theta_0}(x) + J_{\theta_0}(x)\Delta\theta$. For brevity, we subsequently denote both cases by J , with the understanding that the Jacobian is always evaluated at the relevant inputs.

The core mechanism of LSR and its two modes of use are illustrated in Figure 1. Starting from a trained parameter vector θ_0 , the residual vector is linearized with respect to the parameter perturbation $\Delta\theta$, which induces a linear least-squares problem and, consequently, a convex loss landscape. To make direct solvers computationally tractable, LSR restricts $\Delta\theta$ to a low-dimensional subspace, yielding the optimal solution of the reduced linearized problem within this subspace at a manageable computational cost. Importantly, at this stage, the LSR correction is not applied as a nonlinear parameter update. Instead, LSR evaluates the linearized solution at the same linearization point to define a refined predictor, thereby improving accuracy without assuming global validity of the linear approximation.

For supervised learning and data-driven operator learning tasks dominated by data-misfit losses, a single one-shot LSR is typically sufficient to expose additional attainable accuracy beyond that reached by conventional gradient-based training. In such settings, further nonlinear alignment of the LSR solution remains essentially a standard data-fitting problem and is generally no easier than fitting the original target, so iterative refinement offers limited additional benefit. By contrast, for operator-constrained problems governed by composite objectives—such as PDE solving—the optimization landscape is often highly nonlinear and severely ill-conditioned. In this regime, iterative LSR becomes effective by alternating linearized refinement with nonlinear alignment, thereby reformulating a difficult residual minimization problem into a sequence of more numerically benign supervised fitting steps anchored at successive one-shot LSR solutions. Rather than serving as a post-training correction, iterative LSR functions as a restructuring of the training process that mitigates the conditioning issues induced by nonlinear operators and physical constraints.

If θ_0 is a first-order stationary point of the residual minimization problem of the full training set, the linearized model admits no descent direction, and consequently one-shot LSR yields a zero correction. This behavior is expected and reflects the fundamental limitation of first-order information at stationarity. In practice, however, gradient-based training rarely reaches such stationary points within realistic computational budgets, even for convex problems induced by local linearization, a phenomenon repeatedly observed in our numerical results. As a result, nontrivial correctable components typically remain in the Jacobian-induced correction space, allowing LSR to consistently improve upon trained models and, in some cases, to reach accuracy levels that are inaccessible to the original nonlinear parametrization. A more detailed discussion of stationarity, zero-update behavior, and the role of linearized correction spaces is provided in Section S4 of the Supplementary Information.

In the following sections, we demonstrate how this unified framework enables consistent, often order-of-magnitude accuracy improvements across a range of learning paradigms, and how direct solver-based refinement exposes accuracy limits that are not reached by gradient-based optimization under standard training procedures. All experiments reported in this paper are conducted on a single NVIDIA A100 GPU with 40 GB of memory.

Example 1 | Function approximation

We begin with a standard two-dimensional function approximation problem to access the attainable accuracy of trained neural networks and to examine the behavior of LSR in the simplest supervised learning setting. The target function is $q(x, y) = \sin(\pi x) \sin(\pi y)$, defined on the square domain $[-1, 1] \times [-1, 1]$, and is approximated using a conventional feed-forward neural network. Network parameters are trained using the Adam optimizer with mini-batches until the test mean squared error (MSE) reaches a clear plateau. To isolate the numerical limits of gradient-based training, this experiment is conducted in an idealized supervised setting with dense, noise-free data and

sufficient model capacity, so that representation error and data noise do not constitute the dominant sources of error. Full details of the network architecture and training procedure are provided in Section S2.1 of the Supplementary Information.

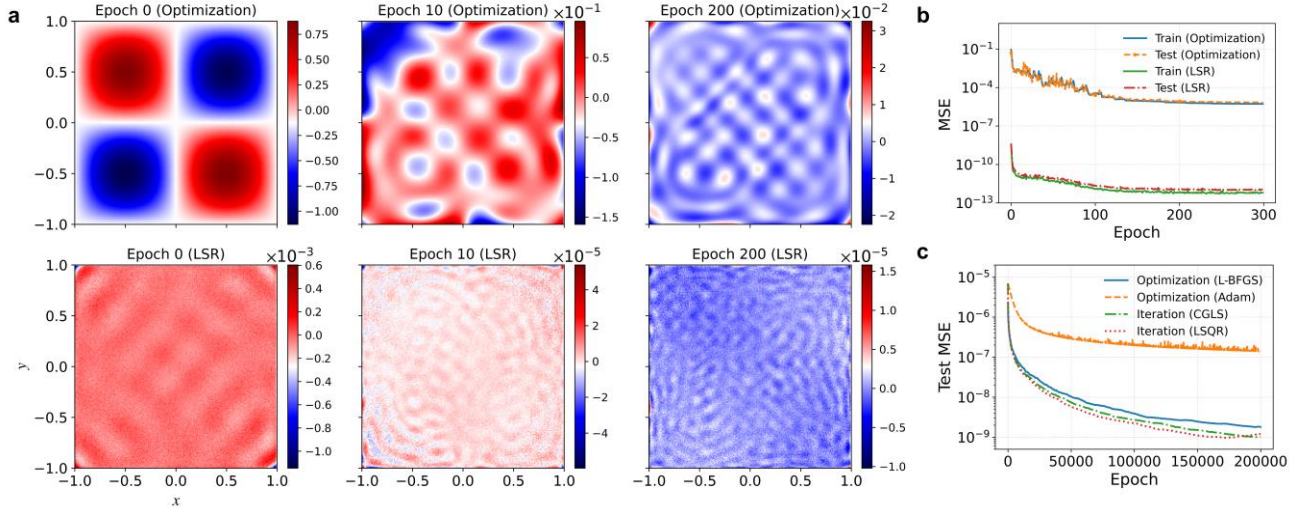


Figure 2 | Accuracy enhancement and characteristic behavior of LSR in a two-dimensional function approximation problem. **a**, Spatial distribution of the network prediction error at different training stages, together with the prediction error after applying one-shot LSR at the same parameter states. **b**, Evolution of the MSE during training. Curves labeled “LSR” indicate the error levels attained by applying one-shot LSR to the network parameters at the corresponding training epochs. **c**, Error convergence for the convex least-squares problem obtained from local linearization of the residual, solved using different optimization or iterative methods.

Figure 2a shows the spatial distribution of the prediction error at different training epochs (0, 10 and 200), together with the error obtained by applying one-shot LSR to the network parameters at the same parameter states. As training progresses, gradient-based optimization progressively suppresses low-frequency error components, while the remaining discrepancy becomes increasingly dominated by high-frequency oscillations, consistent with the well-known spectral bias of neural network training [24,25]. In contrast, one-shot LSR markedly reduces the error magnitude, leaving predominantly fine-scale oscillatory structures. This comparison indicates that, for this simple supervised task, standard training effectively captures the dominant low-frequency content of the target function, whereas the additional accuracy exposed by LSR primarily arises from correcting localized high-frequency errors.

The evolution of the training and test MSE during optimization is shown in Figure 2b. The curves labeled “LSR” report the MSE level obtained by applying one-shot LSR to the network parameters at the corresponding training epoch. Although gradient-based training rapidly reduces the error at early stages, progress slows substantially once a plateau is reached. By contrast, one-shot LSR consistently produces order-of-magnitude MSE reductions throughout training. Notably, even when applied to an

untrained network with random initialization, one-shot LSR attains a prediction accuracy substantially exceeding the eventual plateau reached by gradient-based training. When applied in the plateau regime, one-shot LSR further reduces the test MSE from approximately 10^{-6} to nearly 10^{-12} . In this setting, the wall-clock cost of one-shot LSR is negligible relative to training, requiring less than one second in our implementation.

To further elucidate the origin of this accuracy limitation, Figure 2c examines the least-squares problem obtained by locally linearizing the residual at the trained network state. In this experiment, no subspace reduction is performed; instead, the full-space linearized least-squares problem is solved using different iterative approaches, including first-order Adam, quasi-second-order Limited-memory Broyden–Fletcher–Goldfarb–Shanno (L-BFGS), as well as classical Krylov solvers for least-squares problems, namely Conjugate Gradient for Least Squares (CGLS) and LSQR. It is important to note that the LSR solution, obtained by solving a reduced least-squares problem within a low-dimensional Jacobian-induced subspace, yields a conservative estimate of the achievable error reduction, since the reduced subspace is a strict subset of the full parameter space. Despite the fact that the objective is convex, the accuracy achieved by these iterative methods within a practical iteration budget remains significantly lower than that achieved by the direct solve of the reduced problem. Among the iterative approaches, L-BFGS performs noticeably better than first-order Adam, reflecting partial access to curvature information, while CGLS and LSQR achieve accuracy comparable to L-BFGS. Additional results under different optimizer hyperparameter settings are provided in Section S2.1 of the Supplementary Information.

Taken together, these results highlight a critical yet often underappreciated point: even in the absence of nonconvexity, numerical ill-conditioning alone can constitute a decisive bottleneck for attainable accuracy. Since nonlinear optimization is locally well approximated by a convex problem near a trained solution, this observation further suggests that similar accuracy limitations can persist in nonlinear models, independent of nonconvex effects. This behavior will be further examined and substantiated in more complex problems presented in the subsequent sections.

It is worth emphasizing that the LSR correction is not applied as a nonlinear parameter update. Although the linearized least-squares problem admits a solution with substantially lower residual, applying the corresponding correction direction to the nonlinear model does not yield comparable improvements, as illustrated in Figure S9. Instead, one-shot LSR uses the linearized solution to define a refined predictor evaluated at the same linearization point.

Example 2 | Data-driven operator learning

We next examine the behavior of LSR in a data-driven operator learning setting based on the one-dimensional Burgers equation. The task is to learn the operator mapping from the initial condition $q(x, t = 0)$ to the solution at a later time $q(x, t = 1)$, where the initial conditions are sampled from a

Gaussian random field. Two representative neural operator architectures, DeepONet [2] and MultiONet [26], are considered, together with three different activation functions (ReLU, Tanh, and a custom Tanh–Sin activation), in order to assess the robustness of LSR across network architectures and activation-induced nonlinear representations. All models are trained using standard supervised learning to obtain baseline solutions, after which one-shot LSR is applied as a post-training refinement.

Figure 3a reports aggregate statistics over six operator-learning configurations, combining different architectures and activation functions. Unless otherwise specified, all reported test errors are measured using the relative L_2 norm. Across all settings, LSR consistently reduces the test error compared with the baseline predictions, with the paired distributions revealing systematic accuracy gains across individual test instances rather than isolated improvements. Importantly, instances with lower baseline errors tend to exhibit smaller post-LSR errors, indicating that LSR amplifies—rather than replaces—the benefits of effective nonlinear training. These results demonstrate that the benefits of LSR are robust across architectures and activations, and are not restricted to a small subset of favorable cases.

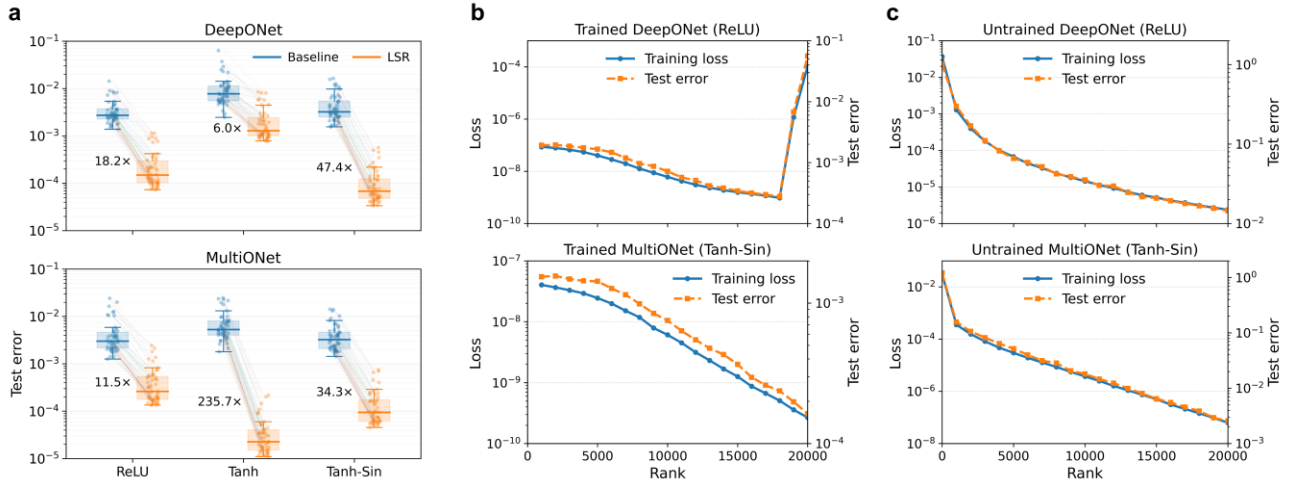


Figure 3 | Accuracy gains from linearized subspace refinement in data-driven operator learning. **a**, Aggregate error statistics over six data-driven operator-learning configurations. Each point corresponds to one of 50 test instances, with paired distributions comparing baseline predictions and their LSR counterparts. Reported numbers indicate the median error reduction factors. **b**, Rank-dependent training loss and test error for representative trained DeepONet and MultiONet models. Increasing the subspace dimension allows LSR to progressively expose lower attainable error levels beyond those reached by gradient-based training. **c**, Corresponding rank-dependent behavior for randomly initialized networks, included as a reference to demonstrate that the Jacobian-induced linear subspace already possesses substantial representational capacity even prior to training.

Figures 3b and 3c further elucidate how these gains depend on the dimension (rank) of the Jacobian-induced linearized subspace. For representative trained DeepONet and MultiONet models

(Figure 3b), increasing the subspace dimension leads to a pronounced and sustained reduction in both training loss and test error. This monotonic trend over a wide range of ranks indicates that the accuracy improvements provided by LSR do not arise from correcting only a few dominant parameter directions. Instead, they reflect the progressive exploitation of additional correction directions admitted by the linearized model as the subspace expands. The corresponding results for randomly initialized networks (Figure 3c) reveal that, even prior to training, the Jacobian-induced linear subspace already possesses substantial representational capacity. As the rank increases, LSR is able to systematically reduce the error, albeit to a higher attainable error floor than in the trained case. This comparison highlights the role of training in reshaping the structure of the linearized subspace, thereby enabling LSR to expose significantly lower accuracy limits, rather than merely providing an optimization pathway.

To further examine the generality of this observation beyond function approximation and operator-learning settings, we additionally tested LSR on the MNIST benchmark [27] using randomly initialized convolutional neural networks. Even without any prior training, applying LSR increases the test accuracy from approximately 0.10 to above 0.96, providing further evidence that the Jacobian-induced linear subspace can already exhibit strong representational capacity at initialization. This result corroborates the consistency of the phenomenon observed in Figure 3c across architectures and at a larger problem scale, with further details provided in Section S2.5 of the Supplementary Information.

At sufficiently large ranks, the monotonic improvement with increasing subspace dimension may eventually deteriorate, with loss and error exhibiting abrupt increases. This behavior reflects the onset of severe numerical ill-conditioning in the reduced linearized least-squares problem as the subspace grows, amplifying sensitivity to noise and finite-precision effects. Consequently, enlarging the subspace introduces an inherent trade-off between increased corrective degrees of freedom and numerical stability, leading to an optimal finite rank for one-shot LSR. Importantly, this instability is directly manifested in the loss behavior itself, providing a practical criterion for rank selection as the largest dimension for which the loss decreases monotonically. In addition to numerical conditioning, the memory cost associated with storing rank-dependent subspace representations provides a practical constraint on the maximum rank used in LSR. Further details are provided in Section S2.2 of the Supplementary Information.

Taken together, these results show that, in data-driven operator learning, the attainable accuracy exposed by LSR is primarily governed by the dimension of subspace. Once the subspace becomes sufficiently expressive, one-shot LSR can approach the optimal solution in the local linearized sense without modifying the network architecture or extending training, whereas excessive subspace expansion is ultimately limited by numerical ill-conditioning.

Example 3 | Fine-tuning physics-informed operator learning

Unlike data-driven operator learning, physics-informed operator learning does not rely on explicit labeled data. Instead, supervision is provided directly through the governing equations together with initial and boundary conditions. As a result, the residual vector is naturally defined at a given prediction instance, rather than over an entire dataset. This structural distinction fundamentally alters how LSR is applied: in physics-informed settings, one-shot LSR can be performed directly on a single predicted solution by constructing the corresponding physical residual and solving a locally linearized correction problem. In this sense, one-shot LSR naturally operates as an instance-wise post-training refinement.

We evaluate this instance-wise one-shot LSR strategy on a collection of widely used benchmark physics-informed operator learning problems introduced by Wang et al. [28]. The benchmarks span a range of representative governing equations, including linear ordinary differential equations, reaction-diffusion systems, the Burgers equation, and advection equations, with uncertainty arising from random forcing terms, source terms, initial conditions, or spatially varying coefficients. In all cases, we adopt the original network architectures and training procedures to obtain baseline models, and then apply a single LSR step to the trained networks without any additional training. Quantitative results are summarized in Table 1. Across all benchmarks, one-shot LSR consistently reduces the physics residual loss at a small additional computational cost and yields stable improvements in test error, with error reductions ranging from approximately one to two orders of magnitude. These results demonstrate that, even in fully label-free and physics-constrained operator learning problems, one-shot LSR serves as an effective post-training refinement framework that exposes accuracy unattained by standard training.

Table 1 | One-shot LSR refinement results for physics-informed operator fine-tuning. All reported results are averaged over 300 instances. Loss denotes the composite physics residual loss used during training, and test error is evaluated against reference solutions.

Governing law	Equation form	Random input	Baseline Loss	Baseline test error	LSR loss	LSR test error	Error reduction factor	Wall time (s)
Linear ODE	$\frac{dq}{dx} = u(x)$	Forcing terms	$3.7 \times 10^{-5} \pm 4.2 \times 10^{-5}$	$3.7 \times 10^{-3} \pm 3.5 \times 10^{-3}$	$2.3 \times 10^{-10} \pm 2.0 \times 10^{-10}$	$1.5 \times 10^{-5} \pm 1.3 \times 10^{-5}$	~240	0.04
Diffusion reaction	$\frac{\partial q}{\partial t} = D \frac{\partial^2 q}{\partial x^2} + kq^2 + u(x)$	Source terms	$6.9 \times 10^{-5} \pm 5.6 \times 10^{-5}$	$5.6 \times 10^{-3} \pm 2.6 \times 10^{-3}$	$8.5 \times 10^{-7} \pm 8.3 \times 10^{-7}$	$5.7 \times 10^{-4} \pm 2.8 \times 10^{-4}$	~10	0.37
Burgers'	$\frac{\partial q}{\partial t} + q \frac{\partial q}{\partial x} - \nu \frac{\partial^2 q}{\partial x^2} = 0$	Initial conditions	$6.7 \times 10^{-4} \pm 5.2 \times 10^{-3}$	$1.2 \times 10^{-2} \pm 1.5 \times 10^{-2}$	$8.6 \times 10^{-9} \pm 3.9 \times 10^{-9}$	$3.9 \times 10^{-4} \pm 2.2 \times 10^{-3}$	~30	6.90
Advection	$\frac{\partial q}{\partial t} + u(x) \frac{\partial q}{\partial x} = 0$	Variable coefficients	$4.9 \times 10^{-3} \pm 4.4 \times 10^{-3}$	$2.2 \times 10^{-2} \pm 6.7 \times 10^{-3}$	$3.1 \times 10^{-5} \pm 2.6 \times 10^{-5}$	$3.1 \times 10^{-3} \pm 9.0 \times 10^{-4}$	~8	6.11

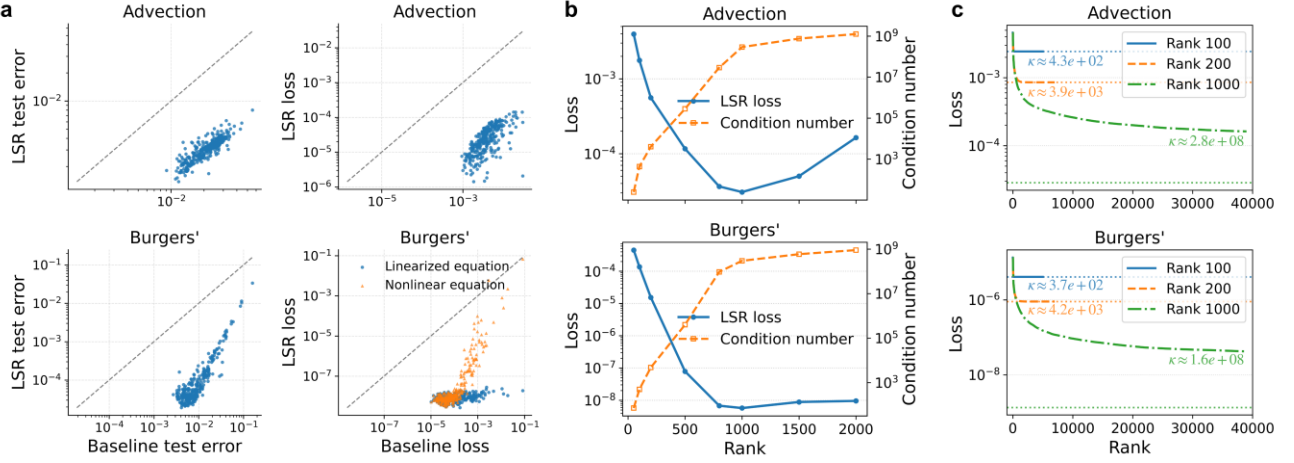


Figure 4 | One-shot LSR behavior and conditioning effects in physics-informed operator fine-tuning. **a**, Baseline and one-shot LSR prediction errors and losses for two representative equations evaluated across 300 prediction instances. **b**, Dependence of the one-shot LSR loss and the condition number of the reduced linearized least-squares system on the linearized subspace dimension (rank), averaged over 300 prediction instances. **c**, Convergence histories of full-batch L-BFGS applied to the reduced linearized least-squares problems at different ranks for representative instances. Horizontal reference lines indicate the loss levels achieved by the corresponding LSR solutions.

To further understand the behavior and limitations of one-shot LSR in physics-informed operator learning, we analyze its performance across different prediction instances and linearized subspace dimensions, as shown in Figure 4. In Figure 4a, we compare baseline and LSR errors and losses for two representative equations, advection and Burgers. For the advection equation, one-shot LSR reliably reduces both error and loss across different instances. In contrast, for the Burgers equation, instances with larger baseline prediction errors tend to retain relatively large errors after LSR, exhibiting a strong correlation between baseline and LSR errors. Importantly, in physics-informed problems, LSR minimizes the linearized physical residual, and when the current prediction deviates substantially from the true solution of a nonlinear equation, the linearized residual can differ significantly from the original nonlinear residual. As a result, a substantial reduction in the linearized residual does not necessarily translate into a commensurate reduction in prediction error, a discrepancy that is clearly reflected in the loss comparison in Figure 4a.

Figure 4b reveals a clear trade-off between subspace expressiveness and numerical stability. As the dimension of the linearized subspace (rank) increases, the LSR loss initially decreases rapidly, but rises again beyond an optimal range. In contrast, the condition number of the associated reduced least-squares system grows monotonically and sharply with rank. Consistent with this trend, Figure S5 shows that the norm of the subspace solution vector increases rapidly with rank and closely follows the growth of the condition number, indicating heightened sensitivity to numerical perturbations. These

results confirm that the observed loss degradation at large ranks is driven by severe ill-conditioning of the reduced linear system.

Finally, Figure 4c provides direct evidence for the origin of the accuracy plateaus observed in gradient-based optimization. For a representative prediction instance, we solve the reduced linearized least-squares problems obtained at the same trained network state using full-batch L-BFGS at different ranks, and compare the resulting convergence histories with the accuracy achieved by direct LSR solves, shown as horizontal reference lines. When the rank is small and the system remains moderately conditioned, L-BFGS converges to essentially the same accuracy level as the corresponding direct solution. However, as the rank increases and the condition number deteriorates, L-BFGS exhibits pronounced stagnation at substantially higher error levels and fails to approach the accuracy attained by the direct solve within a practical number of iterations. Taken together, these results demonstrate that, even though the linearized problems are convex, the attainable accuracy of iterative optimization methods is fundamentally constrained by severe numerical ill-conditioning, rather than by nonconvexity.

Example 4 | PDE solving

In the preceding examples, LSR was employed as a one-shot post-training refinement to unlock attainable accuracy within the local linearized subspace of a trained model. For learning problems with composite loss structures—such as PDE solving—the objective typically couples equation residuals, boundary conditions, and auxiliary constraints. Such objectives are typically highly nonlinear and often severely ill-conditioned, making direct minimization via gradient-based optimization substantially more challenging than supervised fitting. To address this optimization difficulty, we consider an iterative extension of LSR, termed Iterative Linearized Subspace Refinement (I-LSR), which progressively refines the solution by alternating linearized correction with nonlinear alignment.

Within the I-LSR framework, each iteration consists of two stages. First, a one-shot LSR is applied to the linearized residual at the current network, yielding a refined prediction q_{LSR} . Second, the network parameters are updated through a nonlinear alignment step, in which the neural network is driven to approximate q_{LSR} within its parametric representation. In the context of PDE solving, this alignment step should not only bring the network output close to q_{LSR} but also keep the governing equation residual sufficiently small. To this end, we adopt the time-stepping-oriented neural network [29] (TSNN) loss during nonlinear alignment. From a physical viewpoint, this loss can be interpreted as advancing a pseudo-time step using q_{LSR} as the initial value. This perspective converts the original ill-conditioned residual minimization into a sequence of optimization problems with more favorable numerical properties, enabling the network to absorb the LSR results while preserving reduced equation residuals.

Figure 5a shows the evolution of loss and error during I-LSR for the Poisson and Burgers

equations, separating the effects of the LSR and the nonlinear alignment steps. Each iteration consists of one LSR followed by a nonlinear alignment stage, implemented using L-BFGS with 300 and 500 gradient updates for the Poisson and Burgers cases, respectively. At each iteration, the LSR step rapidly reduces both loss and error to their subspace-optimal values. By contrast, during the subsequent nonlinear alignment—except in the first few iterations when the error remains large—the loss and error typically remain well above the corresponding LSR results. This indicates that, under a limited optimization budget, the network cannot fully absorb the LSR results within a single alignment step. Nevertheless, repeated alternation between linearized refinement and nonlinear alignment leads to a consistent reduction in the overall error.

Figure 5b compares the convergence behavior of I-LSR with gradient-based PDE solvers, including PINNs and TSONN. For both the Poisson and Burgers problems, I-LSR reaches low error levels within only a few iterations, demonstrating markedly accelerated convergence. Star markers at the ends of the PINNs and TSONN curves indicate the results obtained by applying an additional one-shot LSR after training. The comparable final accuracies suggest that the primary advantage of I-LSR lies not in substantially lowering the final accuracy reached, but in greatly reducing the optimization effort required to reach high accuracy through systematic alternation of linearized refinement and nonlinear alignment.

The working mechanism of I-LSR is further illustrated by the prediction error distributions for the Poisson equation in Figure 5c. After the initial one-shot LSR applied to an untrained network, the error is dominated by high-frequency oscillations, indicating that the dominant low-frequency components have been effectively removed by LSR. During the subsequent nonlinear alignment step, as the network approximates q_{LSR} , the error structure shifts toward predominantly low-frequency components. Applying LSR again further reduces the error while reintroducing a high-frequency-dominated error, and the following nonlinear alignment step once more transfers the error toward lower frequencies. This alternating pattern highlights the complementary roles of the two stages: LSR performs direct and efficient correction within the local linearized subspace, whereas nonlinear alignment is constrained by network optimizability and cannot fully attain the linearized optimum.

Although nonlinear alignment cannot reproduce the ideal LSR result within a single iteration, repeated alternation of linearized refinement and nonlinear alignment nonetheless yields higher overall accuracy and markedly accelerated convergence. Rather than resolving ill-conditioned residual minimization in a single optimization step, I-LSR leverages this complementary coupling to substantially improve the numerical efficiency and robustness of neural network solvers.

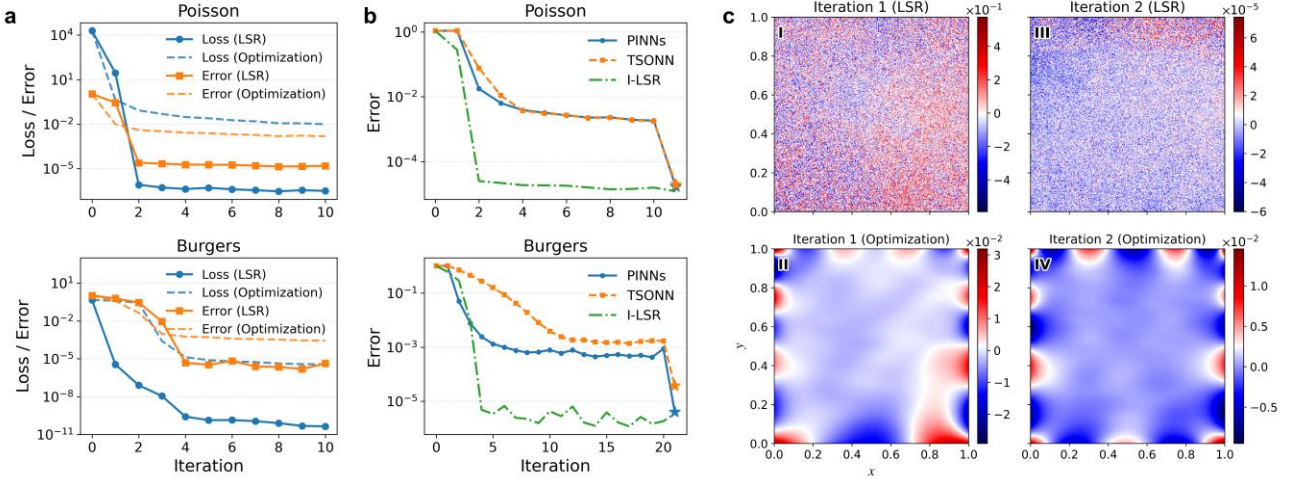


Figure 5 | Convergence behavior and error structure of Iterative Linearized Subspace Refinement (I-LSR) for PDE solving. **a**, Evolution of loss and prediction error during I-LSR iterations for the Poisson and Burgers equations. Each iteration consists of one-shot LSR followed by a nonlinear alignment step. **b**, Comparison of convergence behavior between I-LSR and gradient-based PDE solvers, including PINNs and TSONN. Star markers denote the results obtained by applying an additional one-shot LSR to the trained models. **c**, Spatial error distributions illustrating the alternating error structure during I-LSR for the Poisson equation.

3 Discussion

Accessing attainable accuracy beyond gradient-based training

This work reframes accuracy improvement in neural networks from a perspective complementary to prolonged gradient-based training. Rather than further updating parameters, we study the accuracy that remains accessible at a fixed trained network state through corrections confined to a Jacobian-induced, low-dimensional linearized subspace. This formulation also allows the attainable accuracy of training to be examined within a convex least-squares setting by contrasting the accuracy reached by iterative, gradient-based optimization with that obtained via direct solvers on the same linearized residual problem. Systematic discrepancies between the two provide an indirect diagnostic for identifying locally accessible accuracy that remains unexploited by standard nonlinear training

Within this scope, one-shot LSR targets this subspace and computes a subspace-optimal solution of the locally linearized residual problem via a reduced direct solve. Across function approximation, data-driven operator learning, and physics-informed operator fine-tuning, our results show that this linearized subspace contains substantial accuracy that is difficult to attain through gradient-based training alone. This observation suggests that, in the original nonlinear model, a significant portion of locally accessible accuracy remains unexploited by gradient-based training. Importantly, this attainable accuracy can be systematically recovered by one-shot LSR without modifying network architectures, loss formulations, or training pipelines. In this sense, one-shot LSR serves as a post-training refinement

framework that complements—rather than replaces—existing training methodologies.

Whether further improvement requires Iterative LSR depends on the structure of the learning objective. For tasks dominated by explicit data-misfit losses, one-shot refinement largely saturates the attainable gains, as subsequent nonlinear alignment does not fundamentally alter the problem difficulty. In contrast, for operator-constrained problems with composite objectives—such as PDE solving—Iterative LSR becomes effective by reorganizing training: alternating linearized refinement with nonlinear alignment transforms an ill-conditioned residual minimization into a sequence of numerically more benign supervised fitting problems. This perspective explains the accelerated convergence and stable accuracy improvements observed in practice.

Conditioning-limited accuracy and the role of direct solvers

Beyond the existence of locally attainable accuracy discussed above, our results indicate that numerical conditioning plays a central role in limiting the accuracy reached by gradient-based training. By isolating the reduced linear residual problems defined at fixed trained states, we can examine this effect independently of nonconvexity. Even in these convex least-squares settings, iterative optimization methods may fail to approach the accuracy attainable by direct solvers within a practical computational budget. This gap becomes more pronounced as the effective subspace dimension increases and the associated systems grow more ill-conditioned, reflecting classical conditioning barriers familiar from numerical linear algebra. These observations suggest that a meaningful component of accuracy plateaus in neural network training can be attributed to conditioning-limited optimization, rather than to nonconvexity or representational constraints alone.

Limitations and broader implications

Despite its effectiveness, the LSR framework is subject to several intrinsic limitations. First, the feasibility of direct solvers is constrained by the dimension of the refinement subspace and available computational resources: increasing the subspace rank incurs growing memory and computational costs and can exacerbate numerical ill-conditioning, limiting scalability for very large models or extremely high-dimensional residuals. Second, in settings with noisy observations or insufficient training data, overly large refinement subspaces may amplify noise and induce overfitting, implying that the effective rank should be guided by validation performance rather than computational considerations alone. Finally, while Iterative LSR can substantially improve convergence for operator-constrained problems, its performance ultimately depends on the capacity of the neural network to absorb successive linearized corrections during nonlinear alignment. Iterative refinement does not circumvent fundamental expressivity or optimization limits, but instead reorganizes how these limits are approached.

LSR should be distinguished from Gauss–Newton and Levenberg–Marquardt (GN/LM) methods, which also rely on local linearization of residuals. In GN/LM, the solution of the linearized least-

squares system is interpreted as a parameter update and reinjected into the nonlinear model. LSR, by contrast, does not regard the linearized solution as a valid nonlinear update. As shown in Figure S9, directly applying the LSR correction as a Gauss–Newton or Levenberg–Marquardt step generally fails to reproduce the refined prediction and may even degrade performance. This behavior primarily reflects the breakdown of the local linear approximation when the correction is reinjected into the nonlinear model: the refined linear predictor constructed by LSR often lies outside the narrow region where the first-order expansion remains accurate, and higher-order terms become dominant. This mismatch is further aggravated at large ranks, where the reduced system becomes severely ill-conditioned and the resulting correction can have a large norm (Figure S5), making it particularly unsuitable to be reinjected as a nonlinear parameter update.

An intriguing observation is that substantial accuracy gains can be exposed by LSR even when applied to randomly initialized networks. While such behavior is not intended as a practical learning strategy, it provides diagnostic evidence that Jacobian-induced linear subspaces can already possess considerable expressive capacity at initialization. In this sense, training may be viewed not only as reducing the residual, but also as reshaping the structure of the linearized subspace so that direct refinement methods can access lower attainable error floors. This perspective suggests that LSR may serve as a useful analytical tool for probing the geometry and conditioning of neural network representations, and potentially inform the design of alternative optimization or refinement frameworks.

From a broader perspective, LSR occupies a distinct position among linearized learning paradigms such as extreme learning machines (ELM) [30] and neural tangent kernel (NTK) analyses [31]. ELM employs direct solvers by fixing randomly initialized hidden layers and solving only output-layer weights, which limits hierarchical feature learning. LSR imposes no architectural constraints and instead exploits local linearization around trained states to access the expressive capacity of all parameters. NTK theory characterizes gradient-based convergence via linearized dynamics in the infinite-width limit and is primarily explanatory. In contrast, LSR targets practical finite networks and explicitly seeks to recover attainable accuracy through reduced direct solves. The resulting linear subspaces further provide actionable information on numerical conditioning, offering a concrete basis for analyzing convergence behavior and loss-function design.

4 Methods

Linear residual model

Across supervised regression and classification, data-driven operator learning, and physics-constrained PDE solving, training objectives can typically be expressed in terms of minimizing the norm of a residual vector,

$$\min_{\theta} \frac{1}{2} \|\mathbf{f}(\theta)\|_2^2,$$

where $\mathbf{f}(\theta) \in \mathbb{R}^n$ denotes a residual vector constructed from model predictions evaluated at data samples, observations, or physical constraints. In this work, we focus on a trained parameter state θ_0 and construct a Jacobian-induced linear residual model

$$\mathbf{f}(\theta_0) + \mathbf{G}\Delta\theta, \mathbf{G} \equiv \left. \frac{\partial \mathbf{f}}{\partial \theta} \right|_{\theta_0},$$

with the objective of identifying $\Delta\theta$ that reduces the residual norm within this linearized model.

For notational consistency across learning paradigms, we formally write the Jacobian as $\mathbf{G} = \mathbf{A}\mathbf{J}$, where $\mathbf{J} = \partial \mathbf{q} / \partial \theta$ is the derivative of the network output with respect to parameters, and $\mathbf{A} = \partial \mathbf{f} / \partial \mathbf{q}$ represents the derivative of residuals with respect to outputs. In standard supervised learning, $\mathbf{A} = \mathbf{I}$. In physics-informed learning based on automatic differentiation, however, both \mathbf{f} and \mathbf{q} depend directly on θ , and \mathbf{A} and \mathbf{J} need not be available separately. In practice, only the action of the relevant Jacobian operators is required: the action of \mathbf{J} for constructing the parameter subspace, and the action of the combined operator $\mathbf{G} = \mathbf{A}\mathbf{J}$ for evaluating residual corrections. We therefore retain the notation $\mathbf{A}\mathbf{J}$ without implying that either factor must be explicitly constructed.

Subspace reduction and one-shot LSR

Directly solving the linear residual system in the full parameter space is generally infeasible due to the extremely high dimensionality of θ . We therefore restrict the parameter correction to a low-dimensional subspace,

$$\Delta\theta = \mathbf{V}\mathbf{y}, \mathbf{V} \in \mathbb{R}^{m \times r}, r \ll m$$

where the columns of \mathbf{V} form a linearized subspace basis, capturing parameter directions that most strongly influence variations of the network output at θ_0 .

The subspace basis \mathbf{V} is constructed using randomized singular value decomposition (RSVD). Specifically, a Gaussian random matrix Ω is drawn and the product $\mathbf{J}\Omega$ is computed via Jacobian–vector products. A QR factorization yields an approximate orthonormal basis for the output space, within which a small-scale singular value decomposition of \mathbf{J} is performed to extract the dominant right singular directions, forming the columns of \mathbf{V} .

Restricting the linear residual model to the subspace leads to the reduced linear system

$$\mathbf{A}\mathbf{J}\mathbf{V}\mathbf{y} = -\mathbf{f}(\theta_0)$$

of size $n \times r$. This system is solved using a direct linear least-squares solver (e.g. QR decomposition), yielding the one-shot LSR solution

$$\Delta\theta = \mathbf{V}\mathbf{y}.$$

The entire procedure involves no iterative optimization and does not require explicit formation or storage of \mathbf{J} or \mathbf{G} ; instead, it relies solely on Jacobian–vector products and small-scale linear algebra operations. A detailed summary of the algorithm is provided in Algorithm 1.

Algorithm 1: Linearized Subspace Refinement (LSR)

Input: Trained parameters $\boldsymbol{\theta}_0$, residual function $\mathbf{f}(\boldsymbol{\theta})$, rank r , oversampling parameter p , access to Jacobian–vector products $\mathbf{J}\mathbf{v}$, vector–Jacobian products $\mathbf{J}^T\mathbf{v}$; residual Jacobian–vector products $(\mathbf{AJ})\mathbf{v}$.

1. Evaluate residual vector $\mathbf{f}_0 = \mathbf{f}(\boldsymbol{\theta}_0)$.
2. Draw a Gaussian random matrix $\boldsymbol{\Omega} \in \mathbb{R}^{m \times (r+p)}$, where m is the dimension of parameter vector $\boldsymbol{\theta}_0$.
3. Compute $\mathbf{Y} = \mathbf{J}\boldsymbol{\Omega}$ using Jacobian–vector products.
4. Compute a QR factorization $\mathbf{Y} = \mathbf{QR}$
5. Form the projected Jacobian operator $\mathbf{B} = \mathbf{Q}^T \mathbf{J}$ and compute its SVD $\mathbf{B} = \tilde{\mathbf{U}} \tilde{\boldsymbol{\Sigma}} \tilde{\mathbf{V}}^T$
6. Construct the subspace basis $\mathbf{V} \leftarrow \tilde{\mathbf{V}}(:,1:r)$ (optionally scaled by $\tilde{\boldsymbol{\Sigma}}_r^{-1}$ for preconditioning).
7. Assemble the reduced linearized residual system $\mathbf{AJV}\mathbf{y} = -\mathbf{f}_0$.
8. Solve the reduced system using QR decomposition to obtain \mathbf{y}^* .
9. Set $\Delta\boldsymbol{\theta}^* = \mathbf{V}\mathbf{y}^*$

Output: LSR prediction $\mathbf{q}_{LSR} = \mathbf{q}(\boldsymbol{\theta}_0) + \mathbf{J}\Delta\boldsymbol{\theta}^*$, and LSR residual $\mathbf{f}_{LSR} = \mathbf{f}(\boldsymbol{\theta}_0) + \mathbf{AJ}\Delta\boldsymbol{\theta}^*$

Batch LSR for large-scale datasets

In data-driven operator learning, residuals are often defined over entire training datasets, leading to extremely large residual dimension n . In such settings, intermediate quantities such as $\mathbf{J}\boldsymbol{\Omega}$ and \mathbf{AJV} cannot be formed or stored explicitly at the dataset level. We therefore employ a batch LSR strategy, in which residuals and Jacobian actions are computed over data batches and accumulated in a streaming fashion to assemble the reduced linear system. This approach avoids explicit storage of full dataset–level matrices while preserving the correctness of the reduced linear solve. Implementation details and numerical considerations are provided in Section S1 of the Supplementary Information.

Data Availability

The data used in this study are either obtained from previously published works or generated using the numerical procedures described in the paper. All publicly available datasets are cited in the main text. Any additional data required to reproduce the reported results are provided together with the source code.

Code availability

The code used to generate the results reported in this study is publicly available at <https://github.com/Cao-WenBo/LinearizedSubspaceRefinement>.

Conflict of Interest Statement

The authors have no conflicts to disclose.

Acknowledgments

We would like to acknowledge the support of the National Natural Science Foundation of China (No. 92152301).

References

- 1 Hornik, K., Stinchcombe, M. & White, H. Multilayer Feedforward Networks Are Universal Approximators. *Neural networks* **2**, 359-366 (1989).
- 2 Lu, L., Jin, P., Pang, G., Zhang, Z. & Karniadakis, G. E. Learning Nonlinear Operators Via Deepnet Based on the Universal Approximation Theorem of Operators. *Nature machine intelligence* **3**, 218-229 (2021).
- 3 Karniadakis, G. E. *et al.* Physics-Informed Machine Learning. *Nature Reviews Physics* **3**, 422-440 (2021).
- 4 Raissi, M., Perdikaris, P. & Karniadakis, G. E. Physics-Informed Neural Networks: A Deep Learning Framework for Solving Forward and Inverse Problems Involving Nonlinear Partial Differential Equations. *Journal of Computational Physics* **378**, 686-707 (2019).
- 5 Azizzadenesheli, K. *et al.* Neural Operators for Accelerating Scientific Simulations and Design. *Nature Reviews Physics* **6**, 320-328 (2024).
- 6 Golub, G. H. & Van Loan, C. F. *Matrix Computations*. (JHU press, 2013).
- 7 Trefethen, L. N. & Bau, D. *Numerical Linear Algebra*. (SIAM, 2022).
- 8 Higham, N. J. *Accuracy and Stability of Numerical Algorithms*. (SIAM, 2002).
- 9 LeCun, Y., Bengio, Y. & Hinton, G. Deep Learning. *nature* **521**, 436-444 (2015).
- 10 Goodfellow, I., Bengio, Y., Courville, A. & Bengio, Y. *Deep Learning*. Vol. 1 (MIT press Cambridge, 2016).
- 11 Polyak, B. T. Some Methods of Speeding up the Convergence of Iteration Methods. *Ussr computational mathematics and mathematical physics* **4**, 1-17 (1964).
- 12 Nocedal, J. *Numerical Optimization*. (Springer, 2006).
- 13 Kingma, D. P. Adam: A Method for Stochastic Optimization. *arXiv preprint arXiv:1412.6980* (2014).
- 14 Ioffe, S. Batch Normalization: Accelerating Deep Network Training by Reducing Internal Covariate Shift. *arXiv preprint arXiv:1502.03167* (2015).
- 15 Hagan, M. T. & Menhaj, M. B. Training Feedforward Networks with the Marquardt Algorithm. *IEEE transactions on Neural Networks* **5**, 989-993 (1994).
- 16 Martens, J. in *Icml*. 735-742.
- 17 Lu, L., Meng, X. H., Mao, Z. P. & Karniadakis, G. E. Deepxde: A Deep Learning Library for Solving Differential Equations. *SIAM Review* **63**, 208-228 (2021).

18 Wang, S., Teng, Y. & Perdikaris, P. Understanding and Mitigating Gradient Flow Pathologies in Physics-Informed Neural Networks. *SIAM Journal on Scientific Computing* **43**, A3055-A3081 (2021).

19 Krishnapriyan, A. S., Gholami, A., Zhe, S., Kirby, R. M. & Mahoney, M. W. in *35th Conference on Neural Information Processing Systems (NeurIPS)*. (2021).

20 Wang, Y. & Lai, C.-Y. Multi-Stage Neural Networks: Function Approximator of Machine Precision. *Journal of Computational Physics* **504**, 112865 (2024).

21 Lu, Z., Pu, H., Wang, F., Hu, Z. & Wang, L. The Expressive Power of Neural Networks: A View from the Width. *Advances in neural information processing systems* **30** (2017).

22 Allen-Zhu, Z., Li, Y. & Song, Z. in *International conference on machine learning*. 242-252 (PMLR).

23 Bengio, Y., Louradour, J., Collobert, R. & Weston, J. in *Proceedings of the 26th annual international conference on machine learning*. 41-48.

24 Xu, Z.-Q. J., Zhang, Y. & Luo, T. Overview Frequency Principle/Spectral Bias in Deep Learning. *Communications on Applied Mathematics and Computation* **7**, 827-864 (2025).

25 Zhi-Qin, J., Xu, J., Tao, L., Yanyang, X. & Zheng, M. Frequency Principle: Fourier Analysis Sheds Light on Deep Neural Networks. *Communications in Computational Physics* **28**, 1746-1767 (2020).

26 Zang, Y. & Koutsourelakis, P.-S. Dgno: A Novel Physics-Aware Neural Operator for Solving Forward and Inverse Pde Problems Based on Deep, Generative Probabilistic Modeling. *Generative Probabilistic Modeling* (2025).

27 LeCun, Y., Bottou, L., Bengio, Y. & Haffner, P. Gradient-Based Learning Applied to Document Recognition. *Proceedings of the IEEE* **86**, 2278-2324 (2002).

28 Wang, S. F., Wang, H. W. & Perdikaris, P. Learning the Solution Operator of Parametric Partial Differential Equations with Physics-Informed Deepnets. *Science Advances* **7**, eabi8605 (2021).

29 Cao, W. & Zhang, W. An Analysis and Solution of Ill-Conditioning in Physics-Informed Neural Networks. *Journal of Computational Physics* **520**, 113494 (2025).

30 Huang, G.-B., Zhu, Q.-Y. & Siew, C.-K. Extreme Learning Machine: Theory and Applications. *Neurocomputing* **70**, 489-501 (2006).

31 Jacot, A., Gabriel, F. & Hongler, C. Neural Tangent Kernel: Convergence and Generalization in Neural Networks. *Advances in neural information processing systems* **31** (2018).

Supplementary Information

Wenbo Cao, Weiwei Zhang*

S1. Additional methodological details

S1.1 Choice of subspace basis: output space versus residual space

In the standard LSR formulation presented in the main text, the subspace basis \mathbf{V} is constructed from the Jacobian of the network output $\mathbf{q}(\boldsymbol{\theta})$, that is, by extracting a low-dimensional basis for the column space of $\mathbf{J} = \partial \mathbf{q} / \partial \boldsymbol{\theta}$ using RSVD. For operator-constrained problems, where the residual takes the form $\mathbf{f}(\boldsymbol{\theta})$, one may alternatively construct the subspace from the residual Jacobian $\mathbf{G} = \partial \mathbf{f} / \partial \boldsymbol{\theta} = \mathbf{A}\mathbf{J}$, thereby targeting the residual space directly. In practice, however, we did not observe systematic or practically significant differences in refinement quality between output-space and residual-space constructions. By contrast, constructing the residual-space basis typically incurs a substantially higher computational cost, as it requires repeated Jacobian-vector products involving the composite operator $\mathbf{A}\mathbf{J}$ during subspace construction. For this reason, we recommend constructing \mathbf{V} from the output Jacobian \mathbf{J} in most practical settings.

S1.2 Subspace preconditioning and its effect on solvers

In LSR, the subspace basis \mathbf{V} is optionally preconditioned using the inverse singular values obtained from the reduced SVD, that is, replacing \mathbf{V} by $\mathbf{V}\boldsymbol{\Sigma}^{-1}$. This preconditioning improves the conditioning of the reduced subspace and is equivalent to whitening the dominant Jacobian directions.

Empirically, we observe that this preconditioning has little effect on the accuracy or robustness of direct solvers used in one-shot LSR. However, it can significantly accelerate convergence when gradient-based optimization methods are applied within the reduced subspace. In the main text, where the objective is to isolate and analyze the effect of subspace conditioning on the attainable accuracy of gradient-based training, we therefore deliberately omit this preconditioning when solving reduced linear systems at different ranks. This choice is also conceptually consistent. The preconditioning matrix arises naturally from the reduced-basis construction process, and when no subspace reduction is performed, such a preconditioner is not available.

S1.3 Batch LSR for large-scale datasets

For data-driven operator learning, residuals are often defined over very large training datasets, making it infeasible to form Jacobian-related quantities over the full dataset at once. To address this challenge, we implement a **batch LSR strategy** that evaluates Jacobian actions and assembles the reduced linear system incrementally in a streaming fashion, as shown in Algorithm S1.

Algorithm S1: Batch Linearized Subspace Refinement (batch-LSR)

Input: Trained parameters $\boldsymbol{\theta}_0$, residual function $\mathbf{f}(\boldsymbol{\theta})$, rank r , oversampling parameter p , training data loader, access to Jacobian–vector products $\mathbf{J}\mathbf{v}$, vector–Jacobian products $\mathbf{J}^T\mathbf{v}$; residual Jacobian–vector products $(\mathbf{A}\mathbf{J})\mathbf{v}$.

Step 1: Subspace construction

1. Draw a Gaussian random matrix $\Omega \in \mathbb{R}^{m \times (r+p)}$, where m is the dimension of parameter vector θ_0
2. Initialize an accumulator $\mathbf{H} = \mathbf{0} \in \mathbb{R}^{(r+p) \times m}$
3. For each data batch:
 - Compute $\mathbf{Y} = \mathbf{J}\Omega$ using Jacobian–vector products.
 - Perform a reduced QR decomposition $\mathbf{Y} = \mathbf{QR}$. (If the final batch is smaller than required for QR decomposition due to fixed batch sizing, it is omitted)
 - Accumulate $\mathbf{H} \leftarrow \mathbf{H} + \mathbf{Q}^T \mathbf{J}$.
4. Compute the compact SVD $\mathbf{H} = \tilde{\mathbf{U}} \tilde{\Sigma} \tilde{\mathbf{V}}^T$, and construct the refinement subspace $\mathbf{V} \leftarrow \tilde{\mathbf{V}}(:, 1:r)$ or $\mathbf{V} \leftarrow \tilde{\mathbf{V}}(:, 1:r) \tilde{\Sigma}_r^{-1}$

Step 2: Streaming assembly of the reduced linear system

5. Initialize $\mathbf{R} = \mathbf{0} \in \mathbb{R}^{r \times r}$, $\mathbf{z} = \mathbf{0} \in \mathbb{R}^r$
6. For each data batch:
 - Compute $\mathbf{Y} = \mathbf{AJV}$ using residual Jacobian–vector products, and evaluate the batch residual vector $\tilde{\mathbf{b}} = -\mathbf{f}(\theta_0)$
 - Form the stacked matrix and right-hand side

$$\mathbf{M} \leftarrow \begin{bmatrix} \mathbf{R} \\ \mathbf{Y} \end{bmatrix}, \mathbf{b} \leftarrow \begin{bmatrix} \mathbf{z} \\ \tilde{\mathbf{b}} \end{bmatrix}$$

Compute a reduced QR factorization $\mathbf{M} = \mathbf{Q}_m \mathbf{R}_{new}$

Update $\mathbf{R} \leftarrow \mathbf{R}_{new}$, $\mathbf{z} \leftarrow \mathbf{Q}_m^T \mathbf{b}$

Step 3: Parameter correction

7. Solve the reduced triangular system $\mathbf{R}\mathbf{y} = \mathbf{z}$ to obtain \mathbf{y}^* .
8. Set $\Delta\theta^* = \mathbf{V}\mathbf{y}^*$

Output: LSR prediction $\mathbf{q}_{LSR} = \mathbf{q}(\theta_0) + \mathbf{J}\Delta\theta^*$, and LSR residual $\mathbf{f}_{LSR} = \mathbf{f}(\theta_0) + \mathbf{AJ}\Delta\theta^*$

Once the subspace basis \mathbf{V} is fixed, the batch QR–based assembly and solution of the reduced least-squares problem is mathematically equivalent to the corresponding non-batch formulation using the full dataset, and yields the same reduced normal equations. The use of batch processing only affects the construction of the subspace basis \mathbf{V} , as the Jacobian actions are accumulated incrementally across data batches. In practice, we find that this difference in subspace construction has no noticeable impact on the refinement quality or the attainable accuracy. In addition, although LSR relies on a randomized Gaussian random matrix Ω , we observe very low variance across different random realizations in practice, and therefore do not further elaborate on this aspect.

S1.4 Practical considerations

To reduce memory and computational costs during subspace construction, it is not necessary to use the entire training dataset. It suffices that the residual dimension exceeds the target rank. Empirically, we find that using data batches whose combined residual dimension is approximately $r+1000$ is sufficient to obtain a stable and representative refinement subspace.

In batch LSR, the maximum matrix size—and hence the peak memory footprint—is primarily governed by the parameter dimension m . For very large neural networks, additional memory savings

can be achieved by randomly subsampling network parameters during the construction of the subspace basis \mathbf{V} .

These implementation details ensure that LSR remains scalable and numerically stable for large-scale operator learning problems, while preserving the exactness of the reduced linear problem and the attainable accuracy gains demonstrated in the main text.

S2. Training details and additional results

S2.1 Function approximation

For the function approximation task, we use a fully connected neural network with 6 hidden layers of width 128 and tanh activation functions. The training and test datasets consist of 8,000 and 2,000 randomly sampled points, respectively. Network parameters are optimized using the Adam optimizer, together with a ReduceLROnPlateau learning-rate scheduling strategy. The batch size is set to 32 throughout training. For all LSR experiments in this setting, the refinement subspace dimension is fixed to $r = 1000$.

Figure S1 further shows the train MSE convergence for the convex least-squares problem obtained from local linearization, solved using Adam and L-BFGS optimizers with different hyperparameters. Although the linearized objective is convex and admits an accurate solution via a direct least-squares solve in the reduced subspace, iterative optimization methods exhibit clear accuracy plateaus.

For Adam, larger learning rates yield faster initial convergence, but all tested learning rates converge to nearly identical asymptotic error levels after 10^6 epochs. These asymptotic errors remain orders of magnitude larger than those achieved by the direct solver. For L-BFGS, increasing the history size accelerates early convergence through improved curvature approximation, but does not improve the final attainable accuracy. All tested history sizes converge to similar error levels, again substantially above the direct-solve solution. Together, these results show that even for convex quadratic problems, iterative optimization methods can fail to reach the accuracy accessible to direct linear solvers, highlighting numerical ill-conditioning as a dominant bottleneck.

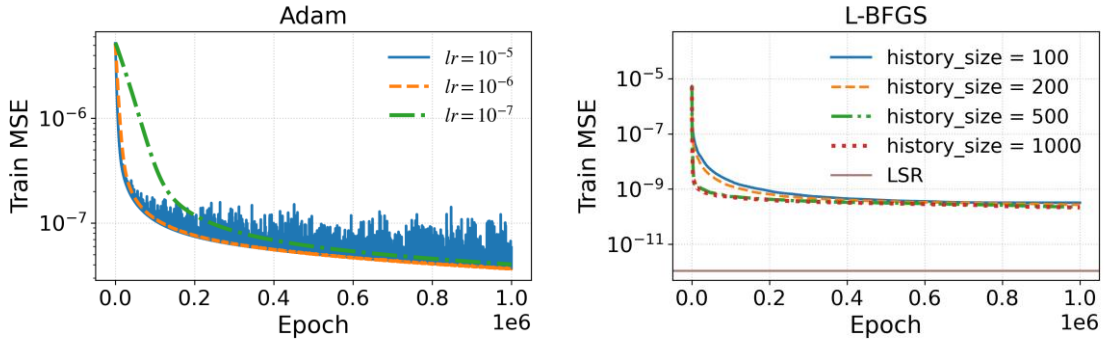


Figure S1. Train MSE convergence for a convex least-squares problem induced by local linearization.

S2.2 Data-driven operator learning

The data-driven operator learning experiments in this section follow the benchmark setup and implementation provided in Ref. [1], together with its publicly available code repository at <https://github.com/yaohua32/Deep-Neural-Operators-for-PDEs/tree/main>. Our modifications are limited to integrating LSR into the existing training and evaluation pipeline.

We consider the one-dimensional, time-dependent viscous Burgers' equation, a standard benchmark for evaluating neural operator methods, $q_t + qq_x = \nu q_{xx}, (x, t) \in [-1, 1] \times [0, 1]$, with initial condition $q(x, t=0) = a(x)$ and periodic boundary conditions. The viscosity coefficient is set to $\nu = 0.1/\pi$. In this setting, the PDE input corresponds to the initial condition, and the learning objective is to predict the final solution $q(x, t=1)$.

The initial conditions are generated by sampling from a Gaussian process $GP(0, 49^2(-\Delta + 49I)^{-2})$, evaluated at 128 uniformly spaced grid points on the interval $[-1, 1]$. Consequently, both the input and output of the neural operator are 128-dimensional vectors. The training dataset consists of 1,000 input–output pairs, and an additional 50 samples are used for testing.

For DeepONet, both the branch and trunk networks are implemented as fully connected networks with four hidden layers of width 128. The MultiONet architecture and associated hyperparameters follow the original code; further details can be found in the corresponding reference and its open-source implementation. In addition to the commonly used ReLU and tanh activation functions, we also consider the Tanh–Sin activation function defined as $\phi(x) = \tanh(\sin(\pi(x+1))) + x$. Additional implementation details are provided in the cited literature and accompanying code.

Figure S2 further reports the loss values and test errors as functions of the subspace rank for all six test cases considered. To reduce memory consumption, only a randomly selected half of the network parameters are used during subspace construction in all experiments. Across different network architectures and activation functions, we consistently observe that LSR yields systematic accuracy improvements, demonstrating its robustness with respect to model design choices.

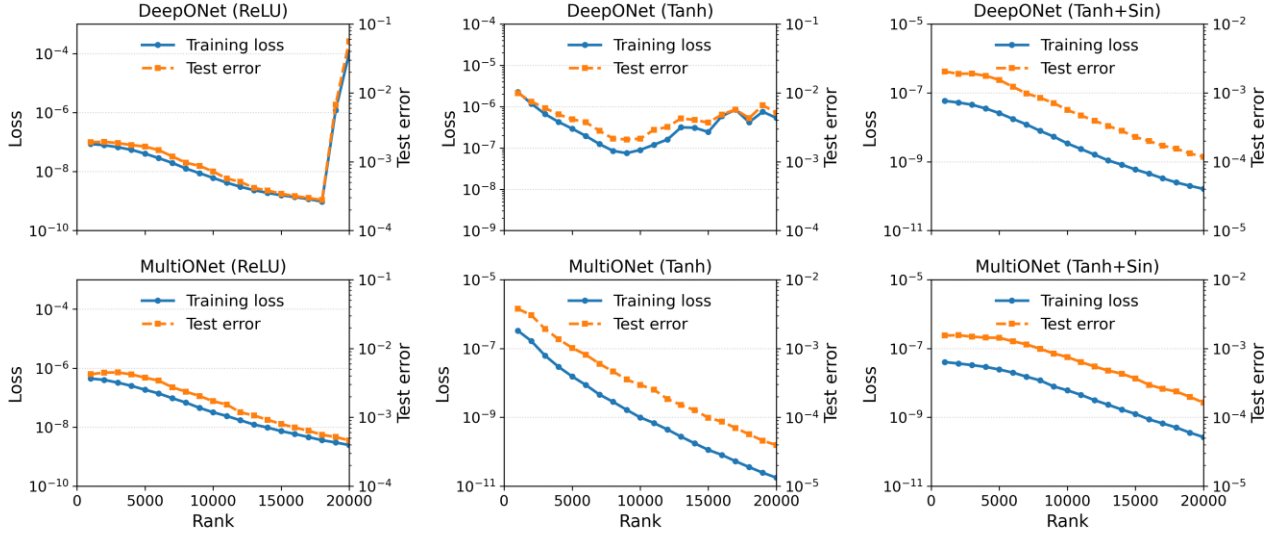


Figure S2. Training loss and test error versus subspace rank for data-driven operator learning.

Figure S3 reports the memory consumption and wall-clock time of LSR as functions of the subspace rank for the two operator learning models, highlighting the extent to which the method is constrained by computational resources. As expected, we observe an approximately linear growth in memory usage with increasing rank, reflecting the storage cost of the reduced subspace and associated linear algebra operations. By contrast, the wall-clock time exhibits a superlinear increase with rank, consistent with the use of direct solvers for the reduced linear systems. These results illustrate the practical trade-offs between attainable accuracy and computational cost when selecting the subspace dimension.

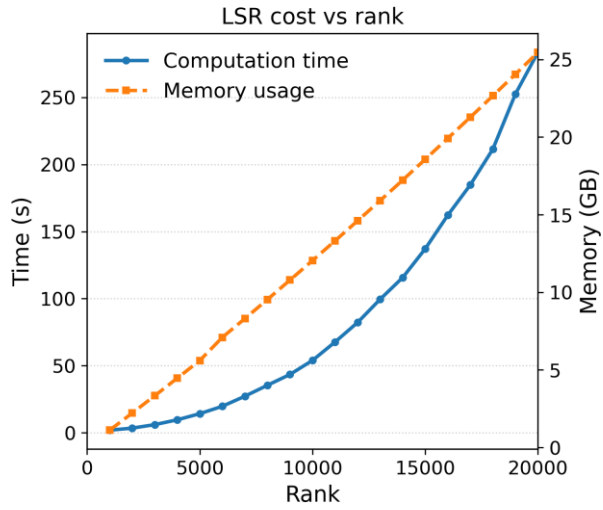


Figure S3. Memory usage and wall-clock time versus subspace rank

S2.3 Physics-informed operator fine-tuning

For the physics-informed operator fine-tuning experiments, all baseline models and training settings follow the configuration reported by Wang *et al.* [2]; detailed descriptions of the problem setup

and training protocols can be found in their original work. Our implementation adopts the same model architectures and optimization strategies, with LSR introduced as an additional refinement step.

For LSR, the subspace rank is selected based on a coarse grid search by identifying the value that yields the lowest average loss over 30 instances. Using this criterion, the resulting ranks for the four equations are rank = 80, 200, 1000, and 800, respectively. Figure S4 presents results for two governing equations that complement those reported in the main text. Across all instances, LSR consistently improves both accuracy and stability relative to the baseline solutions.

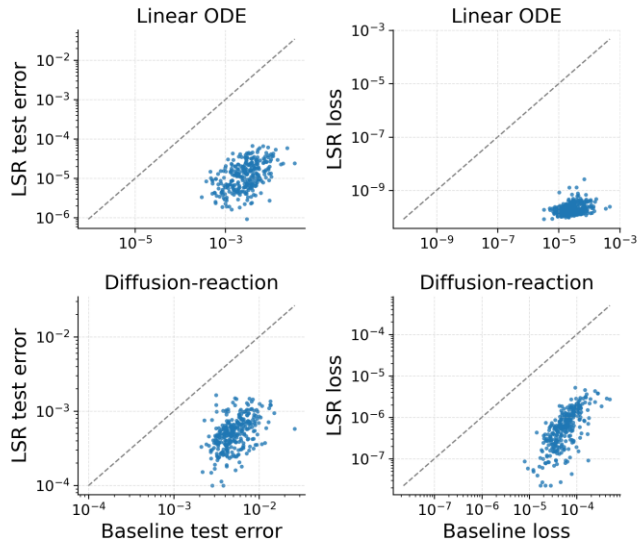


Figure S4. Baseline and LSR results for physics-informed operator fine-tuning.

To further characterize the numerical behavior of the Jacobian-induced subspaces in physics-informed operator fine-tuning, Figure S5 reports how the condition number of the reduced linear system and the norm of the corresponding LSR solution vary with the subspace dimension. The curves are obtained by averaging over 300 representative instances. As the subspace dimension increases, the reduced system becomes progressively more ill-conditioned, as reflected by the rapid growth of the condition number. In parallel, the norm of the reduced-space solution increases, indicating stronger amplification along poorly conditioned directions. Together, these diagnostics provide a quantitative visualization of the subspace-induced ill-conditioning that accompanies higher-dimensional refinements, and motivate the rank-selection discussed in the main text.

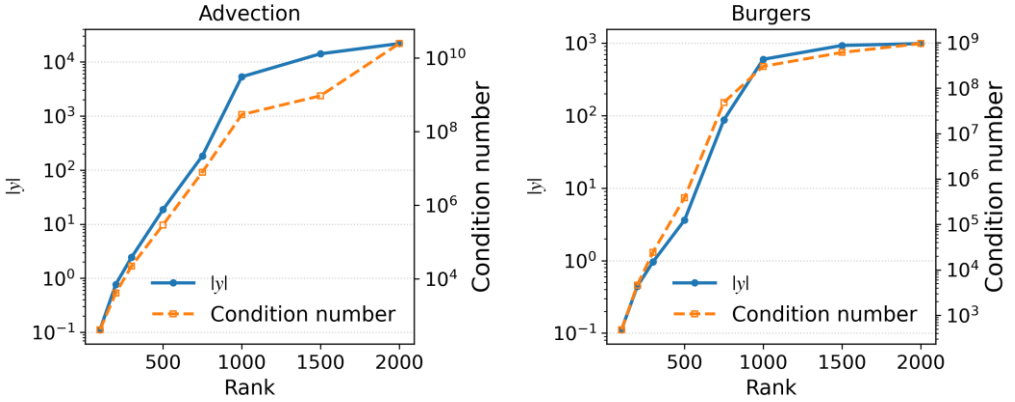


Figure S5. Subspace conditioning and solution norm in physics-informed operator fine-tuning.

To further illustrate the structure of the Jacobian-induced correction subspace, we visualize representative subspace modes for a canonical advection equation example. Figure S6 shows four normalized basis modes corresponding to mode indices 1, 50, 100, and 200. Here, each mode corresponds to the output of the linearized predictor when only a single subspace basis direction is activated, i.e., $\Delta\theta = \mathbf{v}_i$, and the resulting mode is given by the linear response $\mathbf{J}\mathbf{v}_i$. As the mode index increases, the spatial structure of the modes exhibits a clear transition from smooth, low-frequency global patterns to increasingly oscillatory, high-frequency localized structures. The leading modes capture large-scale coherent features of the correction space, while higher-order modes progressively resolve finer spatial variations, providing qualitative insight into the multi-scale nature of the subspace exploited by LSR.

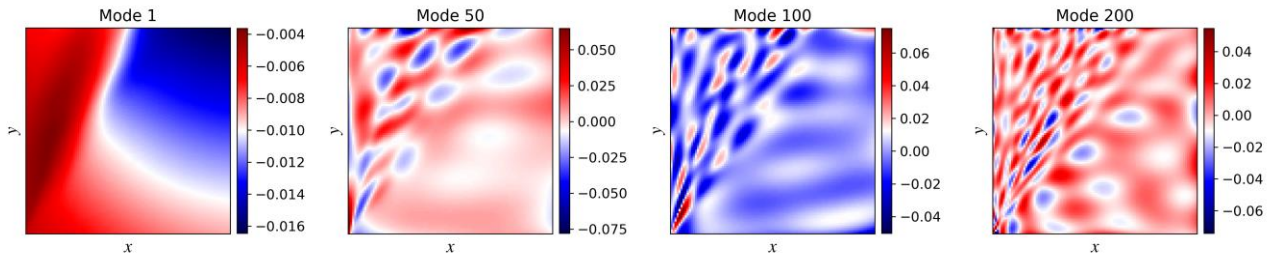


Figure S6. Representative Jacobian-induced subspace modes for the advection equation. Each mode corresponds to the network output induced by activating a single normalized basis vector in the reduced Jacobian subspace.

S2.4 PDE solving

For PDE solving, we consider two benchmark problems: the two-dimensional Poisson equation and the one-dimensional Burgers' equation.

The Poisson equation is defined as

$$q_{xx} + q_{yy} = f_s(x, y), (x, y) \in \Omega = [0, 1]^2$$

where the source term $f_s(x, y)$ and Dirichlet boundary conditions are chosen such that the exact

solution is $q(x, y) = \sin(4\pi x^2) \sin(\pi y)$.

The Burgers' equation is defined as

$$q_t + q q_x + \frac{0.01}{\pi} q_{xx} = 0, (x, t) \in [-1, 1] \times [0, 1],$$

with periodic boundary conditions and initial condition $q(x, t=0) = \sin(\pi x)$.

To apply LSR in PDE solving, the loss function must be written in the form of a residual vector. Accordingly, we define the residual vector by stacking the PDE residuals together with boundary-condition residuals and, when applicable, initial-condition residuals. To ensure compatibility with the TSONN framework, the PDE residual is formulated as

$$(q - q_0) / \Delta\tau - f(q) = 0,$$

where q_0 denotes a reference state and $\Delta\tau$ is a pseudo-time step.

In the LSR step, we take the limit $\Delta\tau \rightarrow \infty$ (implemented numerically as $\Delta\tau = 10^{10}$), which recovers the original PDE residual. During the nonlinear alignment step, which aims to absorb the LSR correction into the neural network, we set $q_0 = q_{LSR}$ and choose $\Delta\tau = 0.3$. This choice enables the network to fit the LSR solution while maintaining sufficiently small PDE residuals, thereby stabilizing the iterative refinement process.

For both PDE problems, we employ fully connected neural networks with six hidden layers of width 128. Residuals are evaluated at 20,000 interior collocation points, and boundary conditions are enforced using 2,000 boundary points. Additional implementation details and training configurations are provided in the accompanying open-source code.

S2.5 MNIST classification with randomly initialized CNN

To further assess the applicability of LSR at a larger problem scale, and to validate the representational capacity of Jacobian-induced linear subspaces even in the absence of training, we consider the standard MNIST handwritten digit classification benchmark. In this classification setting, the network outputs logits $q(x; \theta) \in \mathbb{R}^{10}$, and we define the residual vector as $f(q) = \text{softmax}(q) - \text{onehot}(q)$, so that LSR operates on a locally linearized residual model in the same residual-minimization form used throughout this work.

We adopt a lightweight convolutional neural network composed of two strided convolutional layers followed by a low-dimensional latent projection and a linear classification head. The model contains approximately 110k trainable parameters and is randomly initialized.

Figure S7 reports the test-set generalization behavior of one-shot LSR as a function of the subspace dimension (rank), visualized in terms of 1-accuracy on a logarithmic scale for different activation functions. As the subspace rank increases, LSR yields a monotonic and substantial improvement in test accuracy, rising from approximately **0.10** to above **0.96** at sufficiently large rank.

This result demonstrates that, even for an untrained convolutional network, the Jacobian-induced linear subspace already exhibits strong representational capacity, which can be progressively exploited by enlarging the reduced subspace. Figure S8 summarizes the growth of memory consumption and wall-clock time as the subspace rank increases. Both quantities scale approximately linearly with the subspace dimension. In the present implementation, the observed linear scaling of wall-clock time, rather than the superlinear behavior observed in Figure S3, arises because the dominant computational cost in this example comes from repeated evaluations of Jacobian–vector and vector–Jacobian products over the entire train dataset. This structure suggests that more aggressive parallelization could substantially reduce the wall-clock time, particularly for large datasets.

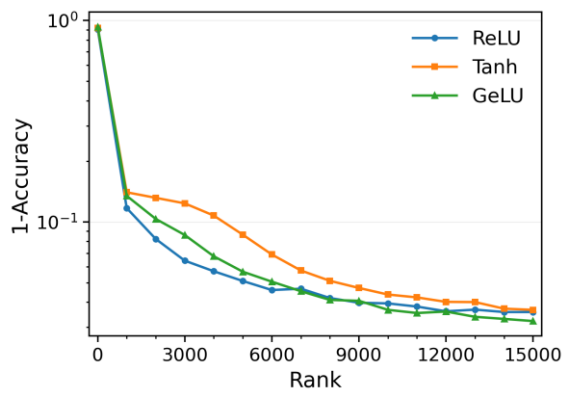


Figure S7. Rank-dependent decay of classification error under LSR for randomly initialized CNNs.

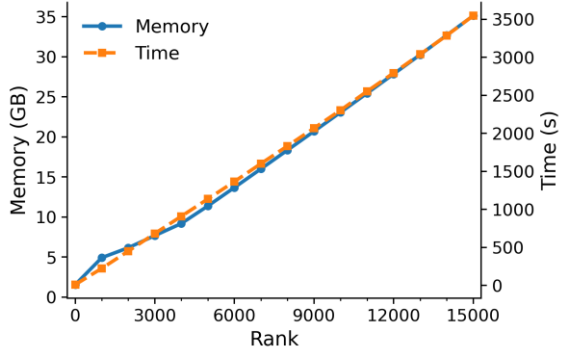


Figure S8. Memory usage and runtime scaling with subspace dimension in batch LSR.

Taken together, these results corroborate the observations in main text from a complementary perspective and at a larger problem scale. They indicate that the expressive power revealed by Jacobian-induced linear subspaces is not limited to operator-learning problems, but also arises in classification tasks with standard convolutional networks. Beyond serving as a post-training refinement tool, this behavior suggests that LSR can be viewed more broadly as a framework for probing and exploiting linearized solution spaces in neural networks, with potential implications for the design and analysis of network architectures.

S3. Interpretation of the LSR correction: linearized refinement versus nonlinear parameter update

This supplementary experiment is designed to clarify the interpretation and intended use of the LSR correction. In particular, we examine whether the correction direction obtained from the linearized least-squares problem can be used as a nonlinear parameter update.

Starting from the same trained network state used in Example 1, we consider the LSR correction direction $\Delta\theta$ obtained by directly solving the reduced linearized least-squares problem. We then evaluate the nonlinear loss along the one-dimensional trajectory $\theta(\alpha) = \theta_0 + \alpha\Delta\theta$ for a range of step sizes α . For comparison, we also evaluate the loss predicted by the linearized model at the same linearization point.

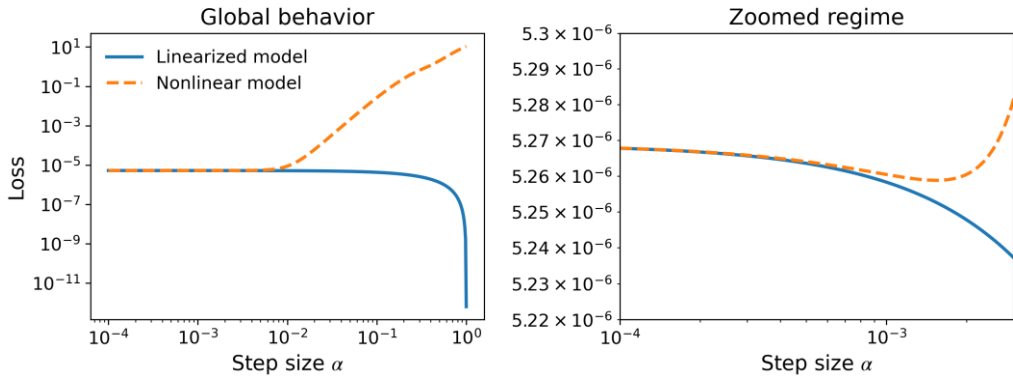


Figure S9. Nonlinear and linearized loss evaluated along the LSR correction direction.

The results are shown in Figure S9. While the loss predicted by the linearized model decreases monotonically along the LSR direction, the nonlinear loss exhibits a markedly different behavior. A slight reduction in the nonlinear loss can be observed only within a very narrow small-step regime, and the magnitude of this improvement is marginal compared with the reduction predicted by the linearized model. As the step size increases, the nonlinear loss rapidly deviates, reflecting the dominance of higher-order terms neglected by the local linear approximation.

These observations indicate that, although the linearized least-squares problem admits a solution with substantially lower residual, the corresponding correction direction does not constitute a reliable descent direction for the original nonlinear objective. Consequently, the LSR correction should not be interpreted as a nonlinear parameter update. Instead, LSR uses the linearized solution to define a refined predictor evaluated at the same linearization point, thereby improving accuracy without assuming global validity of the linear approximation. This observation also helps explain why directly applying local linearization-based update schemes, such as Gauss–Newton or Levenberg–Marquardt methods, can be ineffective or unstable in this setting, as the associated correction directions may not provide reliable descent directions for the original nonlinear objective.

S4. Stationary-point behavior of LSR and a scalar illustrative example

S4.1 Zero correction at first-order stationary points

LSR is derived by linearizing a residual minimization objective around a fixed trained state θ_0 .

Consider the standard nonlinear least-squares problem

$$\min \frac{1}{2} \|\mathbf{f}(\theta)\|_2^2,$$

where $\mathbf{f}(\theta)$ denotes the stacked residual vector and $\mathbf{G} = \partial \mathbf{f} / \partial \theta$ is its Jacobian. The gradient of the objective is $\mathbf{G}^T \mathbf{f}$.

At a first-order stationary point θ_0 , one has $\mathbf{G}^T \mathbf{f} = \mathbf{0}$.

One-shot LSR solves the linearized least-squares problem

$$\min \frac{1}{2} \|\mathbf{f}(\theta) + \mathbf{G}\Delta\theta\|_2^2.$$

The associated normal equations are

$$\mathbf{G}^T \mathbf{G}\Delta\theta = -\mathbf{G}^T \mathbf{f}(\theta_0).$$

Therefore, at a stationary point, the right-hand side vanishes and the linearized problem admits $\Delta\theta = \mathbf{0}$ as a minimizer. In particular, if \mathbf{G} has full column rank on the considered subspace, $\Delta\theta = \mathbf{0}$ is the unique solution; if \mathbf{G} is rank-deficient, any solution must satisfy $\mathbf{G}\Delta\theta = \mathbf{0}$, which yields no change in the linearized prediction and hence no decrease in the linearized residual norm. In either case, one-shot LSR cannot produce a strictly improving correction at a first-order stationary point of the same residual objective.

This behavior is not a failure mode of LSR, but an expected consequence of stationarity: once the first-order optimality condition is satisfied, the local linear model provides no descent direction for the squared residual objective at θ_0 .

S4.2 Why LSR remains effective in practice

The analysis above identifies a clear boundary case: one-shot LSR returns a zero correction when the underlying training has reached a first-order stationary point of the same residual objective. In practice, however, such stationary points are rarely attained under realistic computational budgets, even when the optimization problem is convex. As shown in the main text (Example 1) and further corroborated by the additional function-approximation results in Section S2.1, gradient-based training often stagnates at numerically induced plateaus and remains far from the solution that is accessible by a direct least-squares solve of the corresponding linearized problem.

These observations support the practical regime targeted by LSR: the method is designed to extract additional attainable accuracy at a fixed network state θ_0 when training has not fully satisfied

the stationarity condition $\mathbf{G}^T \mathbf{f} = \mathbf{0}$. In such non-stationary yet stagnated states, the linearized least-squares correction computed by LSR is generally nonzero and can yield consistent refinement.

S4.3 A scalar example illustrating the refined predictor

We next provide a one-dimensional example that visualizes how the linearized predictor family used by LSR can behave differently from the original nonlinear parametric mapping. Here the residual reduces to a scalar for visualization.

Let the scalar model output be

$$q(\theta) = (\theta - 1)^2 + 2,$$

and consider the infeasible target value $q^* = 1$, which corresponds to the desired target output in a supervised neural network fitting setting. Since $q(\theta) \geq 2$ for all θ , the target cannot be matched by the original nonlinear parametric model.

Clearly, when the nonlinear parametric model attains its optimal performance (here at $\theta^* = 1$), linearization at this point yields no meaningful improvement. However, if the nonlinear model has not converged to a stationary point, i.e., $\theta \neq 1$, the linearized model at any such parameter value can render the target $q^* = 1$ attainable by choosing an appropriate $\Delta\theta$, as illustrated in Figure S10.

This simple example highlights two points relevant to LSR. First, the one-shot correction vanishes at stationary points because the linearized model admits no descent direction for the squared residual objective. Second, away from stationarity, the local linearized predictor family anchored at θ_0 can produce corrections that outperform the original nonlinear model, indicating that the linearized model may possess a richer effective expressive capacity than the underlying nonlinear parametric form.

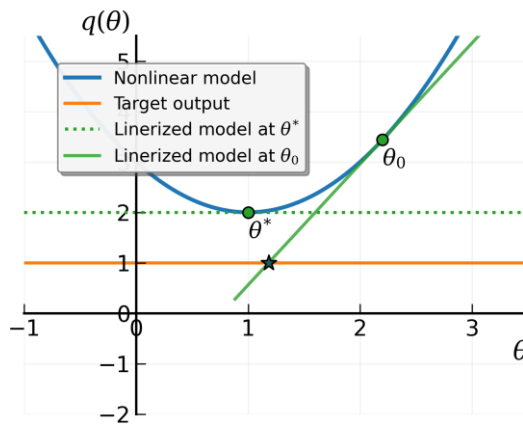


Figure S10. Scalar quadratic example illustrating linearized predictors in LSR.

Probabilistic Modeling (2025).

2 Wang, S. F., Wang, H. W. & Perdikaris, P. Learning the Solution Operator of Parametric Partial Differential Equations with Physics-Informed DeepONets. *Science Advances* **7**, eabi8605 (2021).